Park, J. & Santamarina, J. C. *Géotechnique* [https://doi.org/10.1680/jgeot.17.P.124]

Sand response to a large number of loading cycles under zero-lateral-strain conditions: evolution of void ratio and small-strain stiffness

J. PARK* and J. C. SANTAMARINA†

Geotechnical structures often experience a large number of repetitive loading cycles. This research examines the quasi-static mechanical response of sands subjected to repetitive loads under zero-lateral-strain boundary conditions. The experimental study uses an automatic repetitive loading frame operated with pneumatic pistons. Both vertical deformation and shear wave velocity are continuously monitored during 10 000 repetitive loading cycles. The void ratio evolves towards the terminal void ratio e_T as the number of load cycles increases. The terminal void ratio e_T is a function of the initial void ratio e_0 and the stress amplitude ratio $\Delta\sigma/\sigma_0$. The number of cycles N^* required to reach half of the final volume contraction ranges from $N^* \rightarrow 1$ for densely packed sands ($e_0 \rightarrow e_{min}$) to $N \rightarrow 10^3$ for loosely packed sands ($e_0 \rightarrow e_{max}$). As the soil approaches terminal density at a large number of cycles, peak-to-peak strains are dominated by elastic deformations, and the minute plastic strains that remain in every cycle reflect local and sequential contact events. The shear wave velocity increases during cyclic loading with data suggesting a gradual increase in the coefficient of earth pressure K_0 during repetitive loading. Changes in shear wave velocity track the evolution of the constrained modulus M; in fact, the constrained modulus can be estimated from the shear wave velocity to compute soil deformation in a given cycle. A simple procedure is suggested to estimate the potential settlement a layer may experience when subjected to repetitive mechanical loads.

KEYWORDS: compressibility; creep; deformation; settlement; stiffness; vibration

INTRODUCTION

Geotechnical structures often experience repetitive loading cycles. Previous studies have explored the soil response to all kinds of repetitive loads, including: mechanical cycles associated with wind, waves, pavements, railroads and foundations (Monismith *et al.*, 1975; Poulos, 1989; Jardine, 1991; Brown, 1996; White & Lehane, 2004; Wichtmann *et al.*, 2005, 2010a; Andersen, 2009; LeBlanc *et al.*, 2010; Indraratna *et al.*, 2013; Wu *et al.*, 2017; Guo *et al.*, 2018); chemical cyclic changes in pore fluid (Di Maio, 1996; Musso *et al.*, 2003); thermal cycles (Viklander, 1998; Pasten & Santamarina, 2014; Di Donna & Laloui, 2015); drying and wetting sequences (Albrecht & Benson, 2001; Alonso *et al.*, 2005; Tripathy & Rao, 2009); freeze–thaw cycles (Chamberlain *et al.*, 1990; Viklander, 1998; Qi *et al.*, 2008); and repetitive changes in pore water pressure (Orense *et al.*, 2004; Nakata *et al.*, 2013; Huang, 2016).

The design of geo-structures needs to consider the influence of repetitive loads on long-term performance, serviceability and safety. For example, this applies to energy-related geosystems such as pumped hydro-storage, monopile-supported wind turbines, compressed air energy storage and energy piles (Peng *et al.*, 2006; Andersen, 2009; Pasten & Santamarina, 2011; Sánchez *et al.*, 2014; Loria *et al.*, 2015). The number of mechanical loading cycles in these systems can be particularly high: monopile-supported wind turbines experience more than $N = 10^7$ cycles during a typical design life (Achmus *et al.*, 2009; Li *et al.*, 2015), while tidal cycles exceed $N = 10^4$ in a 30 year design life.

Repetitive mechanical loads can cause significant accumulations of permanent deformations when the cyclic strain exceeds the threshold strain (Brown, 1974; Luong, 1980; Wichtmann *et al.*, 2010b; Pasten *et al.*, 2014); then, there are associated changes in the void ratio, hydraulic conductivity, small-strain stiffness, compression index and friction angle (Youd, 1970; Boulon & Foray, 1986; Uesugi *et al.*, 1989; Kelly *et al.*, 2006; Achmus *et al.*, 2009). Consequently, repetitive mechanical loads can hinder the long-term performance of a variety of geosystems.

The present study explores the mechanical response of sands subjected to repetitive loading under zero-lateral-strain conditions. This paper extends a previous study by the authors (Chong & Santamarina, 2016) to address a large number of load cycles (i.e. $N = 10^4$), various stress amplitude ratios $\Delta\sigma/\sigma_0$ and the analysis of elastic cyclic deformation and the accumulation of plastic strain. The new repetitive loading system designed for this study facilitates automatic stress-controlled repetitive loading cycles and provides small-strain data. Basic concepts are reviewed first, followed by the experimental programme and test results. The discussion provides a procedure for first-order cyclic deformation and cumulative settlement estimates that are valuable for engineering applications.

Manuscript received 8 May 2017; revised manuscript accepted 22 June 2018.
Discussion on this paper is welcomed by the editor.

* Earth Science and Engineering, King Abdullah University of Science and Technology (KAUST), Thuwal, Saudi Arabia (Orcid:0000-0001-7033-4653).
† Earth Science and Engineering, King Abdullah University of Science and Technology (KAUST), Thuwal, Saudi Arabia.

SOIL RESPONSE TO REPETITIVE LOADS: TERMS AND PROCESSES

The analysis and discussion of the long-term response of soils subjected to repetitive mechanical loads require terms and concepts that are not part of the standard geotechnical vocabulary. These concepts and associated observations are briefly introduced and defined next.

Threshold strains

The imposed strain level determines the underlying particle-scale deformation mechanisms. On the one hand, if the strain level is smaller than the elastic threshold strain $\varepsilon_{th}|^{el}$, elastic deformations occur at grain contacts and the fabric remains constant (Vucetic & Dobry, 1991; Vucetic, 1994; Pasten *et al*., 2014). On the other hand, strain accumulations through particle rearrangement and fabric changes take place above the volumetric threshold strain $\varepsilon_{th}|^{v}$ (note: $\varepsilon_{th}|^{v} \approx 30{\cdot}\varepsilon_{th}|^{el}$ – Ishihara, 1996). A theoretical analysis based on the Hertzian contact predicts a lower threshold strain for stiffer particles and at lower confining stresses (Santamarina *et al*., 2001). It remains unclear whether the threshold strain levels obtained under quasi-static loading conditions apply to the soil response under repetitive loading.

Volumetric strain: terminal void ratio

A soil subjected to repetitive loading will reach a stable asymptotic terminal void ratio (D'Appolonia & D'Appolonia, 1967; Narsilio & Santamarina, 2008). The convergence rate towards the terminal void ratio depends on the initial packing density, particle shape, initial stress level and cyclic stress amplitudes (Ko & Scott, 1967; Silver & Seed, 1971; Chong & Santamarina, 2016). The evolution of the void ratio towards an asymptotic terminal state under zero-lateral-strain conditions involves changes in horizontal stress (D'Appolonia *et al*., 1969; Sawicki & Swidzinski, 1995; Wichtmann *et al*., 2010c).

Shear strain: shakedown or ratcheting?

In terms of shear strains, there are two distinct asymptotic trends (Sharp & Booker, 1984; Collins *et al*., 1993; Alonso-Marroquın & Herrmann, 2004; Werkmeister *et al*., 2005; Wu *et al*., 2017). Shakedown takes place when the permanent deviatoric strain accumulation per cycle $\dot{\varepsilon}_d^{acc} = \partial\varepsilon_d^{acc}/\partial i$ vanishes as the number of cycles i tends to infinite, $\dot{\varepsilon}_d^{acc} \to 0$ as $i \to \infty$. On the other hand, ratcheting refers to unceasing deviatoric strain accumulation, $\dot{\varepsilon}_d^{acc} > 0$ as $i \to \infty$.

Loading history

In this study, the effect of repetitive loading on a sand specimen under zero-lateral-strain conditions is investigated. More complex deformation mechanisms may arise in engineering situations where every point in a soil mass experiences different and evolving repetitive loading histories. For example, densification, convective flow cells and ratcheting develop in the complex boundary-valued problem of laterally loaded piles (Cuéllar *et al*., 2009, 2012).

EXPERIMENTAL STUDY: DEVICES AND TEST PROCEDURE

This experimental programme explores the evolution of the void ratio and the small-strain stiffness of sands subjected to repetitive mechanical loads under zero-lateral-strain conditions. The repetitive loading system consists of an instrumented floating-ring oedometer cell and an automatic stress-controlled frame (Fig. 1). The tall floating ring oedometer cell (inner diameter, ID = 52·5 mm, 3·9 mm wall thickness and 100 mm high) is designed to ensure the alignment of the top and bottom caps during repetitive loading (outer diameter, OD = 50·8 mm and 50·8 mm height).

Stress-controlled repetitive loading system

The loading system consists of a rigid reaction frame, pneumatic cylinders and peripheral control electronics.

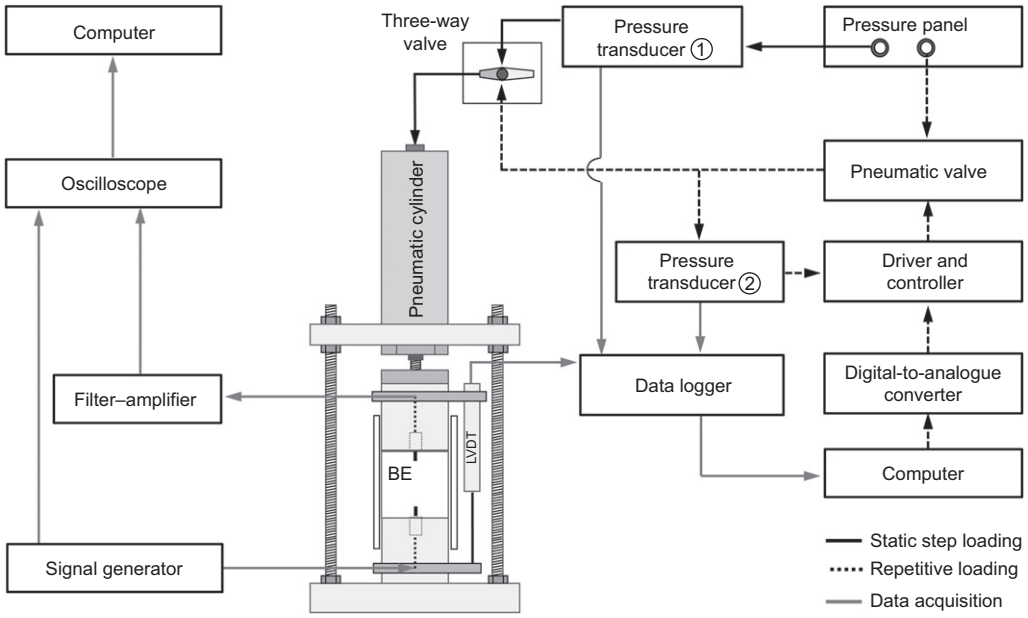

Fig. 1. Device – schematic diagram of the pneumatic system used for static and repetitive loading. The peripheral electronics are used to measure deformation and shear waves. The oedometer cell consists of a floating ring, top and bottom caps with bender elements (BE) and LVDT clamps. Top and bottom cap dimensions: 50·8 mm dia. and 50·8 mm high. Floating ring dimensions: ID = 52·5 mm, OD = 60·3 mm and 100 mm high

The computer sends the digitised command signal to the digital-to-analogue converter (DAC) (Labjack U3-LV). The controller (proportional-integral-derivative controller (PID) – Enfield Technologies C1) activates the pneumatic valve (Enfield Technologies LS-V25s) to match the analogue command signal from the DAC and the analogue signal received from the pressure transducer. The loading system can operate in a strain-controlled mode if the linear variable differential transducer (LVDT) response is used as the feedback signal instead of the pressure transducer.

Deformation monitoring

The LVDT (TransTek DC 0242) clamped to the top and bottom caps tracks the vertical deformation of specimen. LVDT data are saved by the data logger (Keysight 34970A, Fig. 1).

Shear waves: bender elements

The top and bottom caps include bender elements which are mounted inside removable nylon screws. Grounded parallel-type bender elements were used for both the source and receiver to minimise crosstalk (Lee & Santamarina, 2005). The bender elements are 12·7 mm × 8 mm × 0·7 mm in size, and are mounted with a 5 mm cantilevered length (7·7 mm anchored length). The function generator sends a 10 V step signal every 50 ms (Keysight 33210A). Received signals go through a filter-amplifier (Krohn-Hite 3364 – 500 Hz high-pass and 200 kHz low-pass window) before they are averaged in the oscilloscope and stored. (Keysight DSOX 2014A – 1024 stacked signals – see implications of signal stacking in Santamarina & Fratta (2005).)

Selected soil

This experimental study uses Ottawa 20/30 sand (roundness = 0·9; median grain size $D_{50} = 0{\cdot}72$ mm; maximum and minimum void ratios $e_{max} = 0{\cdot}742$ and $e_{min} = 0{\cdot}502$; specific gravity $G_s = 2{\cdot}65$). Previous repetitive load studies using Ottawa sand have explored shear-strain-induced settlements (Youd, 1972), the behaviour of sand–concrete interfaces (Desai *et al.*, 1985), the collapse of sand fabrics associated with liquefaction (Alarcon-Guzman *et al.*, 1988), stiffness characteristics in stress–strain responses (Georgiannou *et al.*, 2008), terminal density (Narsilio & Santamarina, 2008), the effect of density on cyclic behaviour (Georgiannou & Konstadinou, 2014) and plastic strain accumulation models (Chong & Santamarina, 2016). Their results guided the design of this study.

Test procedure

The specimen preparation method involves different tamping energies to attain target relative densities between $D_r = 30$ and 70%. The loading sequence consists of four stages: (*a*) static step loading to σ_0; (*b*) repetitive loading by $N = 10^4$ cycles with amplitude $\Delta\sigma$; (*c*) static loading to the maximum vertical stress; and (*d*) unloading. Loading cycles have a period of $T = 12$ s to avoid dynamic effects ($f = 0{\cdot}083$ Hz). Previous studies have revealed that the loading frequency f does not affect the strain accumulation rate when $f = 0{\cdot}05$ to 30 Hz (Youd, 1972; Shenton, 1978; Tatsuoka *et al.*, 1986; Wichtmann, 2005).

Shear wave measurements during the repetitive loading stage take place at the same vertical effective stress $\sigma_0 + \Delta\sigma$ at the top of cycles $i = 1$, 10, 100, 300, 1000, 3000 and 10 000. Table 1 summarises all test conditions.

Table 1. Test condition

Initial vertical stress, σ_0: kPa	Stress amplitude, $\Delta\sigma$: kPa	Stress amplitude ratio, $\Delta\sigma/\sigma_0$	Initial relative density, D_r* (number of tests)
174	$\Delta\sigma = 138$ ($174 \leftrightarrow 312$)	0·8	40% (3) 70% (3)
105	$\Delta\sigma = 138$ ($105 \leftrightarrow 243$)	1·3	40% (6) 70% (6)
67	$\Delta\sigma = 100$ ($67 \leftrightarrow 167$)	1·5	30% (1) 50% (1) 70% (1)
105	$\Delta\sigma = 276$ ($105 \leftrightarrow 381$)	2·7	40% (3) 70% (3)
105	$\Delta\sigma = 414$ ($105 \leftrightarrow 519$)	4·0	40% (3) 70% (3)

*Note: target value. The measured value is used in all plots and analyses.

EXPERIMENTAL RESULTS

All 33 tests in Table 1 exhibit similar trends. This section presents detailed experimental results for two specimens $D_r = 44\%$ and $D_r = 86\%$, subjected to loading cycles with stress amplitude $\Delta\sigma/\sigma_0 = 1{\cdot}3$ (Table 1). The complete dataset is then analysed in the subsequent section.

Effective stress σ'_z plotted against void ratio e

Figure 2 presents the change in void ratio during the static–repetitive–static loading history followed by the static unloading stage. The void ratio for the loosely and densely packed sands decreases monotonically during the initial static loading stage. The dotted circles indicate creep deformation at a constant load. Repetitive loading cycles cause higher contraction in the looser specimen.

Vertical effective stress σ'_z plotted against strain ε_z

Figure 3 presents the same repetitive load response shown in Fig. 2 in the stress–strain space. The recoverable and irrecoverable strains are clearly seen in the earlier loading–unloading cycles. The plastic strain accumulation becomes negligible as the number of cycles increases, but it remains hysteretic – that is plastic shakedown.

Evolution of void ratio

Figure 4 illustrates the void ratio evolution with the number of cycles for the two specimens reported above ($D_r = 44\%$ and 86%; $\Delta\sigma/\sigma_0 = 1{\cdot}3$). Once again, most changes in void ratio take place in earlier cycles and are more significant in the loosely packed sand. Figs 4(a) and 4(b) show experimental results fitted with a modified accumulation model (see Paute *et al.*, 1993; Chong & Santamarina, 2016)

$$e_i = e_T + (e_1 - e_T)\left[1 + \left(\frac{i-1}{N^*}\right)^m\right]^{-1} \quad \text{for } i \geq 0 \text{ and } m > 0 \tag{1}$$

where the void ratio e_i is measured after the ith cycle, and the void ratio e_1 corresponds to $i = 1$. The fitting parameters include the exponent m and the asymptotic terminal void ratio e_T as $i \to \infty$; the number of cycles is $(1 + N^*)$ when the compaction is half of the asymptotic contraction $(e_1 - e_T)/2$.

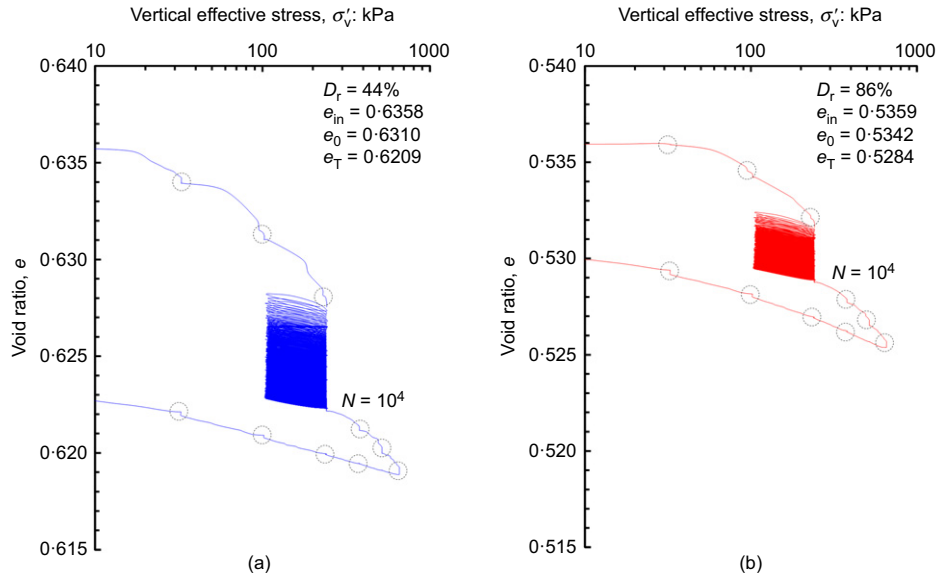

Fig. 2. The change in void ratio during the static–repetitive–static loading history followed by the static unloading sequence: (a) loose sand, $D_r = 44\%$; (b) dense sand, $D_r = 86\%$. Test conditions: $\sigma_0 = 105$ kPa, stress amplitude ratio $\Delta\sigma/\sigma_0 = 1{\cdot}3$ (from 105 to 243 kPa)

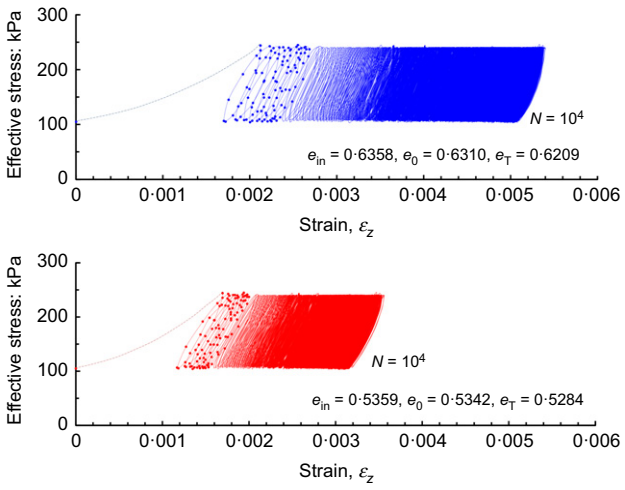

Fig. 3. Stress–strain response during repetitive loading cycles: (a) loose sand, $D_r = 44\%$; (b) dense sand, $D_r = 86\%$. Test conditions: $\sigma_0 = 105$ kPa, stress amplitude ratio $\Delta\sigma/\sigma_0 = 1{\cdot}3$ (from 105 to 243 kPa)

Shear wave signals

Figure 5 shows the shear wave signal cascades recorded during the 'static–repetitive–static' loading history followed by the unloading stage. The travel time decreases during the first quasi-static loading stage. Changes in the first arrival are less obvious during repetitive loading. The present authors use the time-stretched cross-correlation method in Coda wave analysis to assess these minor changes in travel time (Snieder, 2006; Dai *et al.*, 2013). Then, the stretching factor θ allows minute changes in the shear wave velocity to be determined during repetitive loading cycles.

ANALYSES AND DISCUSSION

In this section, the complete dataset produced with the 33 tests run for this study (Table 1) is reported and analysed.

Terminal void ratio and maximum contraction

The terminal void ratio e_T and the characteristic number of cycles N^* describe the soil response to repetitive loads for engineering purposes (equation (1)). Fig. 6(a) shows that the asymptotic terminal void ratio e_T scales with the initial void ratio e_0. In other words, specimens do not evolve to a single soil fabric but retain memory of their initial fabric even after a very large number of cycles (see also López-Querol & Coop, 2012; Chong & Santamarina, 2016). However, the terminal void ratio e_T decreases as the stress amplitude ratio $\Delta\sigma/\sigma_0$ increases (note: this statement applies to soils under zero-lateral-strain conditions, and should not be extended to dilative soils subjected to repetitive deviatoric loads under triaxial conditions). In fact, the dimensionless volume contraction $\lambda = (e_T - e_{min})/(e_0 - e_{min})$ is strongly correlated to the stress amplitude ratio $\Delta\sigma/\sigma_0$ as shown in Fig. 6(b): $\lambda = 1{\cdot}0 - 0{\cdot}05(\Delta\sigma/\sigma_0)$.

The characteristic number of cycles N^* required to reach half of the asymptotic volume contraction $\Delta e = (e_1 - e_T)/2$ increases with the increasing initial void ratio e_0 (Fig. 6(c)); in fact, $N^* \rightarrow 1$ for densely packed sands ($e_0 \rightarrow e_{min}$) and $N^* \rightarrow 10^3$ for loosely packed sands ($e_0 \rightarrow e_{max}$). Less obvious is the fact that N^* also increases with stress ratio $\Delta\sigma/\sigma_0$. This occurs because the terminal void ratio e_T is lower for higher $\Delta\sigma/\sigma_0$, hence, a larger number of cycles is required to attain half of the asymptotic contraction $\Delta e = (e_1 - e_T)/2$. Fig. 6(d) shows that the m exponent is relatively constant, $m = 0{\cdot}45 \pm 0{\cdot}05$. Finally, the number of cycles i_η required to attain a certain η fraction of the ultimate compaction $(e_1 - e_i) = \eta(e_0 - e_T)$ is computed from equation (1)

$$i_\eta = 1 + N^* \left(\frac{\eta}{1-\eta}\right)^{1/m} \tag{2}$$

Maximum change in relative density ΔD_T. The modified accumulation model allows the asymptotic terminal void ratio e_T to be estimated (equation (1) and Fig. 4). Then, the maximum change in relative density $\Delta D_T = (e_0 - e_T)/(e_{max} - e_{min})$ from $i = 0$ to $i \rightarrow \infty$ is a function of the asymptotic contraction $\Delta e = e_0 - e_T$ and the attainable void ratio range e_{max}–e_{min}. The void ratio range e_{max}–e_{min} is selected to generalise these results to other coarse-grained soils subjected to repetitive loads.

Figure 7 plots the maximum change in relative density ΔD_T against the initial relative density $D_{i=0} = (e_{max} - e_0)/(e_{max} - e_{min})$ at $i = 0$ for all specimens and stress amplitude

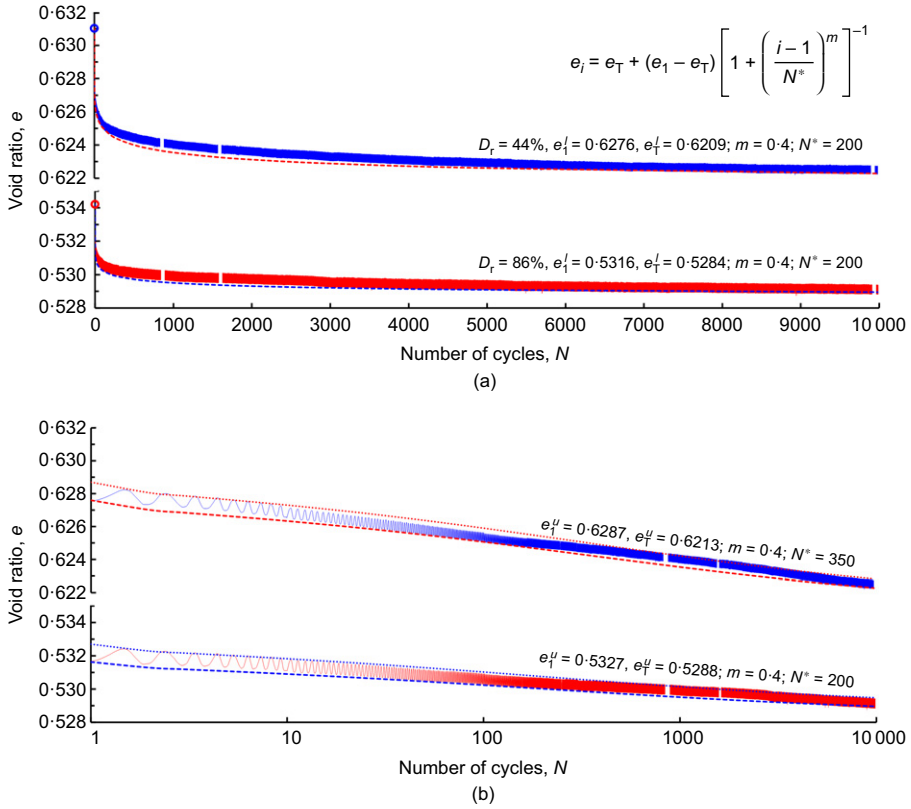

Fig. 4. Void ratio evolution with number of cycles, *i*: (a) linear scale: (b) logarithmic scale. Test conditions: $\sigma_0 = 105$ kPa, stress amplitude ratio $\Delta\sigma/\sigma_0 = 1{\cdot}3$ (from 105 to 243 kPa)

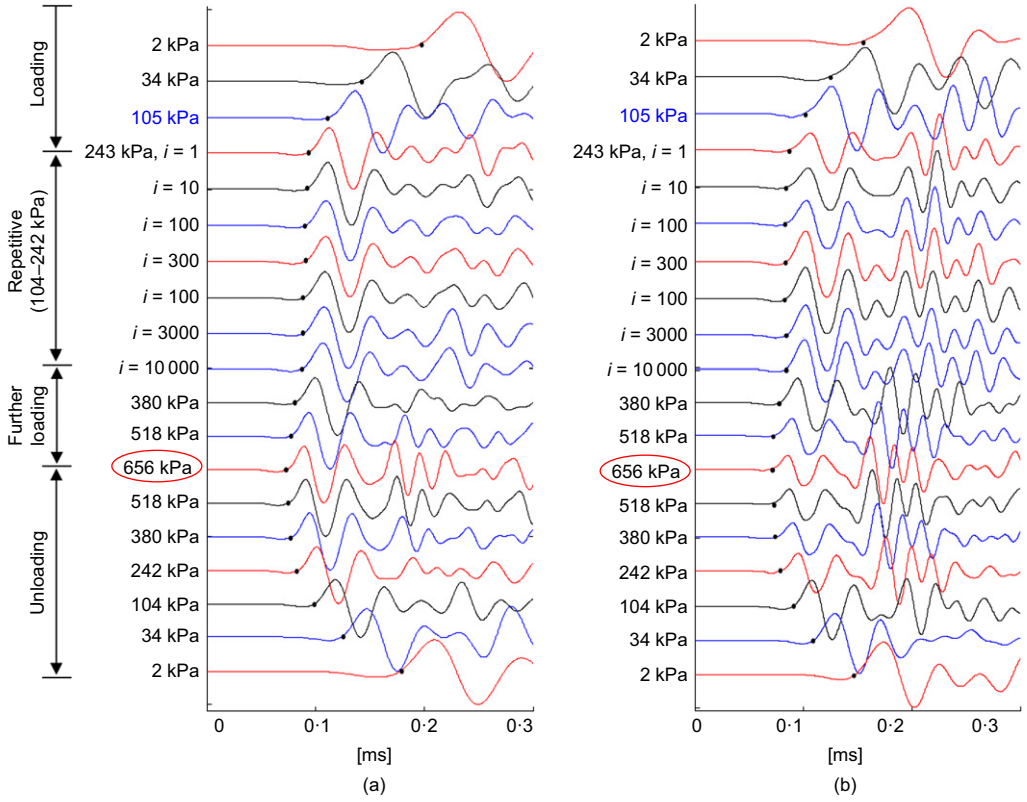

Fig. 5. Cascade of shear wave signals captured during the 'static–repetitive–static' loading history followed by unloading: (a) loose sand, $D_r = 44\%$: (b) dense sand, $D_r = 86\%$. Test conditions: $\sigma_0 = 105$ kPa, stress amplitude ratio $\Delta\sigma/\sigma_0 = 1{\cdot}3$ (from 105 to 243 kPa)

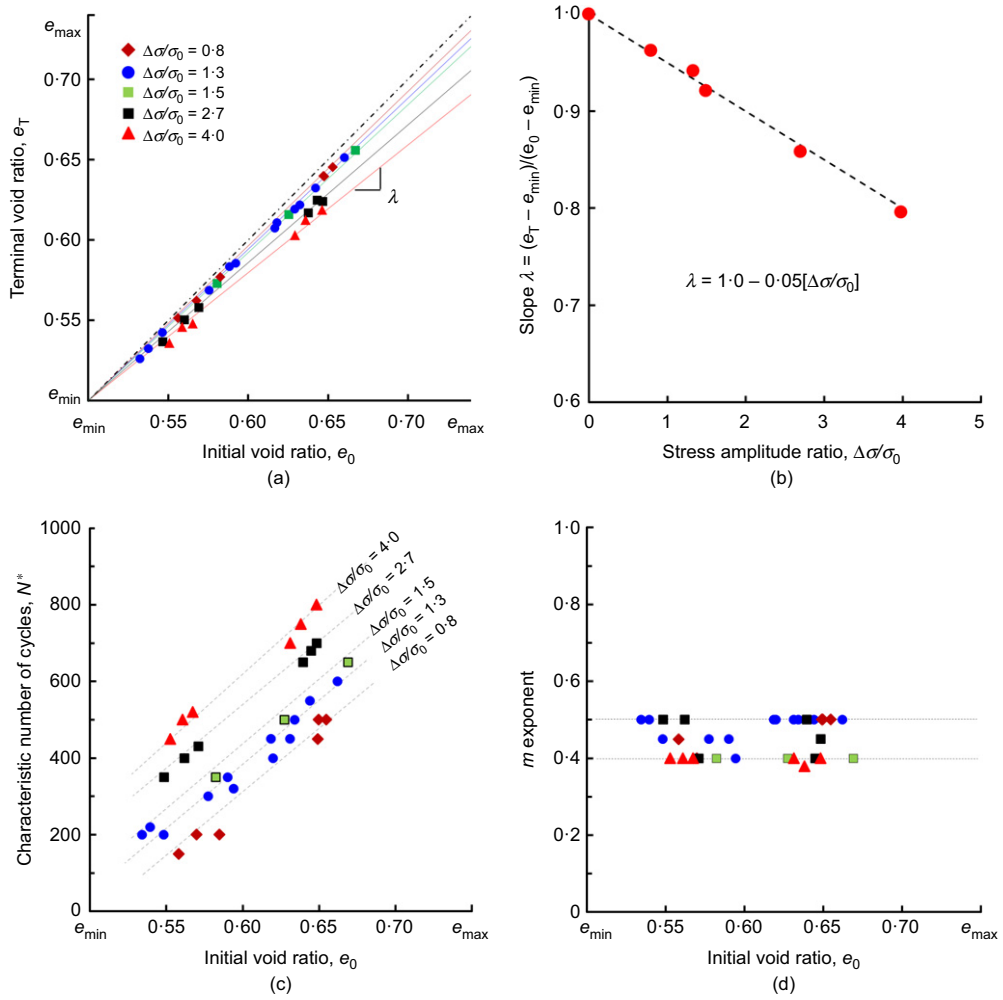

Fig. 6. Terminal void ratio and characteristic number of cycles: (a) terminal void ratio e_T plotted against initial void ratio e_0 for different stress amplitude ratios, $\Delta\sigma/\sigma_0$; (b) slope $\lambda = (e_T - e_{min})/(e_0 - e_{min})$ plotted against stress amplitude ratio, $\Delta\sigma/\sigma_0$; (c) characteristic number of cycles N^* plotted against initial void ratio e_0 as a function of stress amplitude ratio; (d) fitting model parameter m plotted against initial void ratio e_0

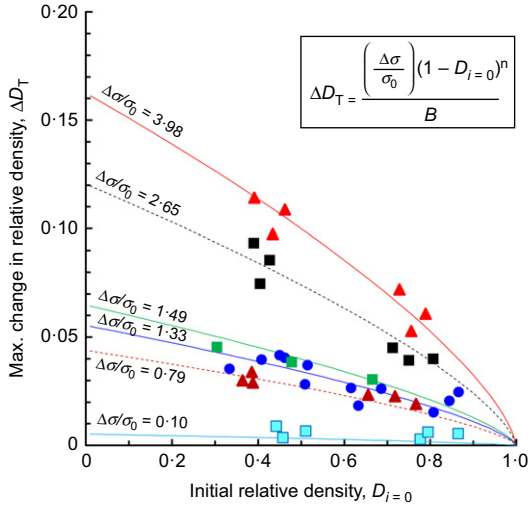

Fig. 7. Estimation of the maximum change in relative density due to repetitive loading. Model parameters: $n = 0{\cdot}7$ (all trends) and $B = 20{\sim}25$. Data for $\Delta\sigma/\sigma_0 = 0{\cdot}10$ extracted from Chong & Santamarina (2016) are superimposed on this figure

ratios $\Delta\sigma/\sigma_0 = 0{\cdot}8$ to 4·0; data for $\Delta\sigma/\sigma_0 = 0{\cdot}10$ extracted from Chong & Santamarina (2016) are superimposed on Fig. 7. Then, assuming no volume contraction when the initial void ratio $e_0 = e_{min}$, the anticipated maximum change in relative density is a function of the stress amplitude ratio and the initial relative density as

$$\Delta D_T = \frac{(\Delta\sigma/\sigma_0)(1 - D_{i=0})^n}{B} \tag{3}$$

In this study, $B \approx 20$ to 25 and $n = 0{\cdot}7$ for all cases.

Strain and particle-scale deformation mechanisms

Strain levels. The plastic strain accumulation per cycle decreases and becomes negligible as the number of vertical K_0 load cycles increases. The first ten loading–unloading cycles illustrated by the dotted line in Fig. 3 highlight both recoverable and irrecoverable deformations.

The upper and lower accumulation model trends fitted to test results e^u and e^l define the peak-to-peak strain in i cycle $\varepsilon_{pp}(i)$ (Fig. 4(b) and equation (1))

$$\varepsilon_{pp}(i) = \frac{\Delta e_i}{1 + e_i} = \frac{e_i^u - e_i^l}{1 + e_i^l} \tag{4}$$

However, the permanent change in void ratio between two consecutive cycles defines the plastic strain $\varepsilon^{pl}(i)$ between the i and $i + 1$ cycles (Fig. 4(b))

$$\varepsilon^{pl}(i) = \frac{e_i^l - e_{i+1}^l}{1 + e_i^l} \tag{5}$$

For example, consider the data shown in Fig. 4. Equation (2) is used to compute the i_η cycle for a target $\eta = 90\%$ of the compaction to terminal density, and equations (4) and (5) to estimate the peak-to-peak strain ε_{pp} and the plastic strain ε^{pl} in the i_η cycle. The dense sand will reach 90% compaction after $i_\eta = 48\,600$ cycles, the peak-to-peak strain in that cycle will be $\varepsilon_{pp} = 3{\cdot}1 \times 10^{-4}$ and the plastic contraction will be $\varepsilon^{pl} = 1{\cdot}6 \times 10^{-9}$; corresponding values for the loose sand are $i_\eta = 85\,000$ cycles, $\varepsilon_{pp} = 2{\cdot}9 \times 10^{-4}$ and $\varepsilon^{pl} = 1{\cdot}8 \times 10^{-9}$. Clearly, elastic deformations dominate the peak-to-peak strain as the specimen evolves towards terminal density at a large number of cycles; particle-scale deformation mechanisms are explored next.

Deformation mechanisms. Particle-scale deformation mechanisms in sands include elastic deformation at particle contacts, particle rotation (when the coordination number is low), contact slippage and crushing (Whitman, 1970; Omidvar *et al.*, 2012). The release of stored strain energy during unloading may also cause contact slippage and yield; consequently elastic strains are not necessarily equal to recoverable strains (Rowe, 1954; Barden & Khayatt, 1966; Daramola, 1980).

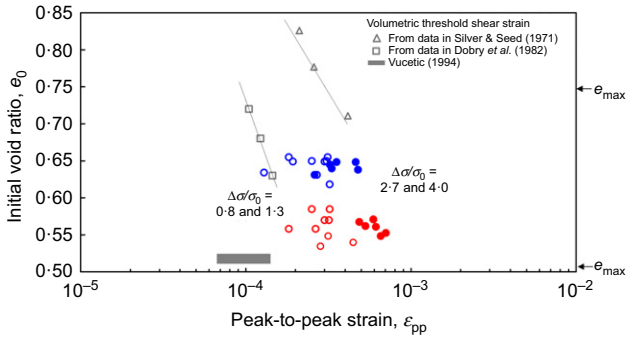

Fig. 8. Peak-to-peak strain ε_{pp} values after $\eta = 95\%$ compaction. Data show the effect of initial void ratio e_0 and stress amplitude ratio $\Delta\sigma/\sigma_0$. The corresponding plastic strains are between $\varepsilon^{pl} = 1 \times 10^{-10}$ and 9×10^{-10} for all tests

Monotonic one-dimensional (1D) compression test results for loose and dense Ottawa sand specimens show that the yield stress is $\sigma_y \approx 20$ MPa (Roberts & de Souza, 1958; Valdes, 2002; Guimaraes *et al.*, 2007). Therefore, the stress levels imposed during repetitive loading in this study are low, $(\sigma + \Delta\sigma)/\sigma_y < 0{\cdot}03$, and grain crushing is disregarded as a primary deformation mechanism. Still, asperity breakage and fretting damage are anticipated (Johnson, 1955, 1961; SEM evidence in Park (2018)).

Figure 8 presents peak-to-peak strains ε_{pp} at $\eta = 95\%$ compaction. The corresponding plastic strains are between $\varepsilon^{pl} = 1$ and 9×10^{-10} for all tests. For comparison, values of the volumetric threshold strain determined during cyclic loading are superimposed on Fig. 8. While the peak-to-peak strain levels are in the range of the threshold strain previously measured for cyclic loading, small plastic strains take place in every cycle. The plastic strain level per cycle is smaller than the strain level that would be required for atomic-scale displacement between contacts $\varepsilon = 0{\cdot}1$ nm/$D_{50} \approx 10^{-7}$. Therefore, as the specimen approaches terminal density, the accumulation of plastic deformation consists of successive, individual contact events (slippage or abrasion) in every cycle, rather than evenly distributed plastic strains throughout the specimen.

Energy loss and stiffness

Damping ratio D *and constrained modulus* M. The damping ratio $D = \Delta W/(4\pi W)$ relates the consumed energy ΔW to the stored energy W in a cycle. However, the constrained modulus in a cycle relates the applied cyclic stress to the peak-to-peak strain $M = \Delta\sigma/\varepsilon_{pp}$.

Figure 9 plots the damping ratio D_i and the constrained modulus M_i against the number of cycles i, where both values D_i and M_i are normalised by the corresponding values in the first cycle, that is D_1 and M_1. For clarity, values are shown at

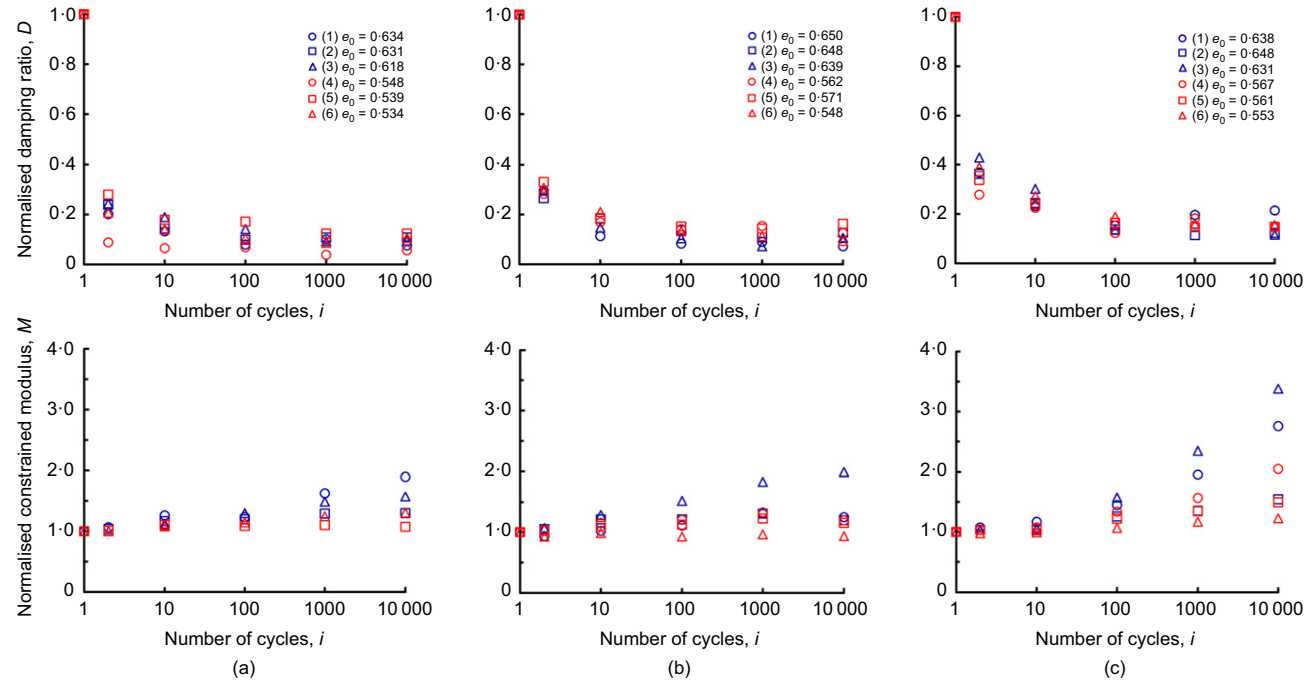

Fig. 9. The evolution in damping ratio D and constrained modulus M plotted against number of cycles for different stress amplitude ratios $\Delta\sigma/\sigma_0$ and for specimens prepared at different initial void ratio, e_0: (a) $\Delta\sigma/\sigma_0 = 1{\cdot}3$; (b) $\Delta\sigma/\sigma_0 = 2{\cdot}7$; (c) $\Delta\sigma/\sigma_0 = 4{\cdot}0$

a selected number of cycles $i = 1$, 2, 10, 100, 1000 and 10 000. The damping ratio decreases while the constrained modulus increases with the number of cycles in all 33 tests. Most of the reduction in the damping ratio takes place in the first few cycles (see also Stokoe *et al.* (1999)), whereas the increase in the constrained modulus continues even after a large number of cycles (see resilient modulus data in Monismith, 2004; da Fonseca *et al.*, 2013). The stress amplitude ratio $\Delta\sigma/\sigma_0$ affects the variation of the constrained modulus as the number of cycles increases. Overall, repetitive mechanical loads result in denser, stiffer and less attenuating sand fabrics under zero-lateral-strain conditions.

Shear wave velocity during static loading. The shear wave velocity is a power function of the vertical σ'_z and horizontal σ'_x effective stresses (vertical propagation, horizontally polarised – Yu & Richard, 1984; Santamarina *et al.*, 2001)

$$V_s = \alpha\left(\frac{\sigma'_z + \sigma'_x}{2\,\text{kPa}}\right)^{\beta} = \alpha\left(\frac{\sigma'_z}{1\,\text{kPa}}\right)^{\beta}\left(\frac{1+K_0}{2}\right)^{\beta} \quad (6)$$

where the α factor is the shear wave velocity at effective stress $\sigma'_{\text{mean}} = 1$ kPa and the β exponent represents the stress sensitivity of the shear wave velocity. The shear wave velocity–stress relation captures both contact behaviour during wave propagation and fabric changes associated with stress changes (Cha *et al.*, 2014).

Figure 10(a) summarises the evolution of the shear wave velocity measured during the static (labelled 1), repetitive (2) and static (3) loading stages for a loose and a dense sand. Fig. 10(b) presents the α factors and β exponents computed by fitting equation (6) to the static load stages before and after repetitive loading for all tests. The data trend is consistent with the relationship between α and β values reported by Cha *et al.* (2014). Overall, the sand becomes stiffer (lower C_c), the α factor increases, the β exponent decreases and the soil fabric becomes less sensitive to stress changes after repetitive loading.

Shear wave velocity during repetitive loading. Small-strain stiffness measurements can be used to estimate the lower bound for the repetitive elastic deformation. Previous studies showed that the small-strain stiffness evolves during repetitive loading cycles (e.g. resonant column: Drnevich & Richart (1970) and Triantafyllidis *et al.* (2004); V_p and V_s: Wichtmann (2005) and Papadopoulos (2014)). Fig. 10(c) presents shear wave velocity data gathered in this study against the number of loading cycles for three loosely packed sands subjected to different stress amplitude ratios $\Delta\sigma/\sigma_0$. The shear wave velocity increases with $\log(i)$ for all stress amplitude ratios $\Delta\sigma/\sigma_0$ (Fig. 10(c))

$$\frac{V_s|_i}{V_s|_1} = i^d \quad (7)$$

The d exponent is a function of the shear wave velocity for the first cycle $V_s|_1$ (Fig. 10(d)). Data points cluster along linear trends for each stress amplitude ratio $\Delta\sigma/\sigma_0$. It is concluded that the rate of increase in small-strain stiffness during repetitive loading is more pronounced in looser and

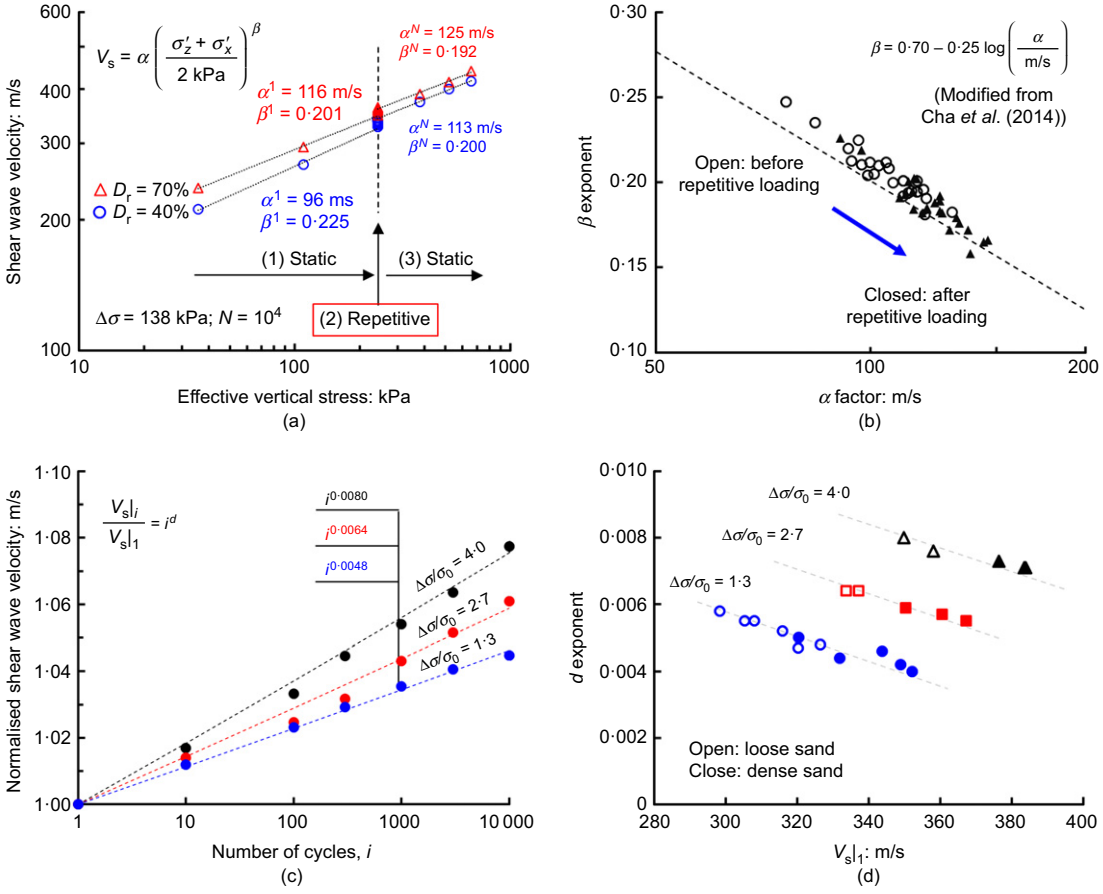

Fig. 10. The evolution of shear wave velocity during static and repetitive loading stages: (a) shear wave velocity plotted against stress; (b) the α factor and β exponent before and after repetitive mechanical loading; (c) normalised shear wave velocity plotted against number of cycles; (d) the d exponent plotted against shear wave velocity at the beginning of repetitive loading, $V_s|_1$

softer sands subjected to high stress cycles; that is, when more significant fabric changes are expected.

Evolution of K_0. The coefficient of earth pressure K_0 at rest relates the in situ horizontal effective stress to the vertical effective stress under zero-lateral-strain conditions (Mayne & Kulhawy, 1982; Talesnick, 2012). The velocity–stress data before and after the repetitive loading stage will now be analysed to estimate the evolution of the coefficient of earth pressure K_0 during repetitive loading. From equation (6)

$$\frac{V_s|_N}{V_s|_1} = \frac{\alpha|_N}{\alpha|_1} \frac{(\sigma'_z|_N/1\,\text{kPa})^{\beta|_N}}{(\sigma'_z|_1/1\,\text{kPa})^{\beta|_1}} \frac{((1+K_0|_N)/2)^{\beta|_N}}{((1+K_0|_1)/2)^{\beta|_1}} \tag{8}$$

Then

$$K_0|_N = \frac{\sigma'_x}{\sigma'_z} = 2\left[\frac{V_s|_N}{V_s|_1}\frac{\alpha|_1}{\alpha|_N}\sigma'^{(\beta|_1-\beta|_N)}_z\left(\frac{1+K_0|_1}{2}\right)^{\beta|_1}\right]^{1/\beta|_N} - 1 \tag{9}$$

Assuming a nominal initial value $K_0|_1 = 0{\cdot}42$, the α and β values fitted before and after repetitive loading allow a stress ratio $K_0|_N \approx 0{\cdot}48 \pm 0{\cdot}02$ to be anticipated immediately after repetitive loading with stress amplitude ratio $\Delta\sigma/\sigma_0 = 1{\cdot}3$. Hence, indirect shear wave velocity measurements suggest a gradual increase in the horizontal stress during repetitive loading under zero lateral strains (see also data in Sawicki & Swidzinski (1995)). From an activation energy perspective, repetitive loads facilitate the development of processes that must overcome an energy barrier, such as friction and particle rearrangement. Related phenomena include time and ageing, heating (in creep), and vibration (rheopexy). During repetitive loading, horizontal stresses are gradually locked in by structural changes and friction, and K_0 increases proportionally to the stress amplitude ratio $\Delta\sigma/\sigma_0$.

Estimation of the constrained modulus from shear wave velocity. The 'mechanistic' method for pavement design uses the resilient modulus to compute elastic deformations (Monismith, 2004; NCHRP, 2004). The resilient modulus $E_r = \sigma_d/\varepsilon_r$ is measured in a triaxial cell and is defined as the ratio between the applied vertical cyclic stress $\Delta\sigma$ and the recoverable axial strain ε_r after a predetermined number of load cycles (Davich *et al.*, 2004). The resilient modulus can be estimated from elastic wave propagation to circumvent measurement difficulties and for the assessment of existing pavements. Published results show that the ratio between the measured resilient modulus and the small-strain Young's modulus computed from the wave velocity is in the range $E_r/E_{max} = 0{\cdot}4$ to $0{\cdot}8$ (Davich *et al.*, 2004; Schuettpelz *et al.*, 2010).

In this study, the ratio M/G_{max} is explored, between the constrained modulus M preferred for 1D deformation analysis and the maximum shear stiffness G_{max} obtained from shear wave velocity (note: M and G_{max} involve different strain levels and they are not related through a single value of Poisson ratio). Fig. 11 presents the M/G_{max} ratio plotted against the number of cycles for different stress amplitudes $\Delta\sigma/\sigma_0$. The stiffness ratio ranges between $1{\cdot}2 \leq M/G_{max} \leq 2{\cdot}3$; lower values apply to denser specimens, M/G_{max} increases with the number of cycles and for lower stress amplitude ratios $\Delta\sigma/\sigma_0$.

Cyclic deformation and maximum settlement

Finally, an estimate will be made of the deformation a layer will experience in a given cycle, as well as the cumulative settlement of the layer when it reaches the terminal void ratio.

The strain in the ith cycle $\varepsilon_i = \Delta\sigma/M$ is the ratio between the cyclic stress amplitude $\Delta\sigma$ and the constrained modulus M, which can be estimated from shear wave velocity measurements in the field, as indicated earlier (Fig. 11). Then, a layer of thickness H will deform $\delta = H\Delta\sigma/M$.

The maximum cumulative strain ε_T as $i \to \infty$ is estimated from the initial and the terminal void ratios $\Delta e = e_0 - e_T$ (refer to results in Figs 6(a) and 6(b))

$$\varepsilon_T = \frac{e_0 - e_T}{1+e_0} = (1-\lambda)\frac{e_0 - e_{min}}{1+e_0} = a\frac{\Delta\sigma}{\sigma_0}\frac{e_0 - e_{min}}{1+e_0} \tag{10}$$

where $a = 0{\cdot}05$ for the sand tested in this study (Fig. 6(b)). Then, the settlement S_T of a layer thickness H subjected to repetitive mechanical loading under zero-lateral-strain conditions is

$$\begin{aligned} S_T &= \int_0^H \varepsilon_T \mathrm{d}z = \int_0^H \frac{e_0(z) - e_T(z)}{1+e_0(z)}\mathrm{d}z \\ &= \int_0^H a\frac{\Delta\sigma(z)}{\sigma_0(z)}\frac{e_0(z) - e_{min}(z)}{1+e_0(z)}\mathrm{d}z \end{aligned} \tag{11}$$

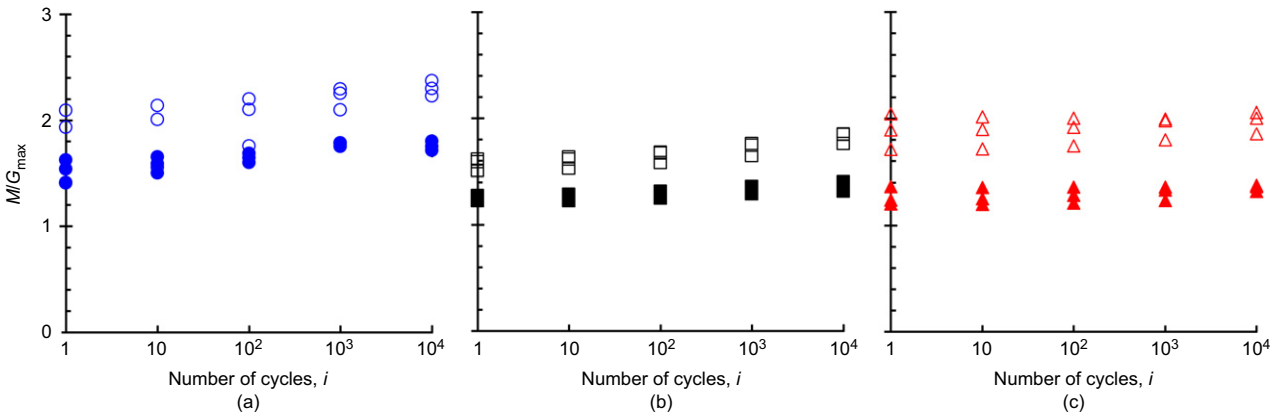

Fig. 11. The ratio between the constrained modulus M and the maximum shear stiffness G_{max} – evolution with the number of cycles for different stress amplitude ratios: (a) $\Delta\sigma/\sigma_0 = 1{\cdot}3$; (b) $\Delta\sigma/\sigma_0 = 2{\cdot}7$; (c) $\Delta\sigma/\sigma_0 = 4{\cdot}0$. Note: open symbols indicate loose specimens (initial relative density $D_{i=0} = 35$ to 51%) and closed symbols indicate dense specimens ($D_{i=0} = 62$ to 88%)

These equations highlight the importance of the initial e_0 and terminal e_T void ratios. Furthermore, the terminal void ratio is readily estimated from e_{min} and the stress amplitude ratio $\Delta\sigma/\sigma_0$. For example, consider a large footing on a homogeneous sandy sediment ($e_{max} = 0{\cdot}74$, $e_{min} = 0{\cdot}50$, $e_0 = 0{\cdot}60$, $a = 0{\cdot}05$). The footing applies σ_0 $(z = 0) = 100$ kN/m^2 and $\Delta\sigma = 50$ kN/m^2. From Figs 6(a) and 6(b) and equation (11), the settlement expected for an $H = 5$ m thick layer is $S_T = 5{\cdot}7$ mm.

CONCLUSIONS

The void ratio, the state of stress, and the small-strain stiffness of sands change during quasi-static repetitive mechanical loads under zero-lateral-strain conditions. Notable conclusions from this study are listed below.

(*a*) The void ratio evolves towards the terminal void ratio e_T as the number of load cycles $i \rightarrow \infty$. The terminal void ratio e_T is a function of the initial void ratio e_0 when repetitive loads take place under zero-lateral-strain conditions. In other words, the soil retains a memory of its initial fabric.

(*b*) The characteristic number of cycles N^* required to reach half of the asymptotic volume contraction $\Delta e = (e_1 - e_T)/2$ increases with an increasing initial void ratio e_0; in fact, $N^* \rightarrow 1$ for densely packed sands ($e_0 \rightarrow e_{min}$), and $N \rightarrow 10^3$ for loosely packed sands ($e_0 \rightarrow e_{max}$).

(*c*) As the soil approaches terminal density at a large number of cycles, peak-to-peak strains are dominated by elastic deformations, and the plastic strains are much smaller than the strain level required for atomic-scale displacement between contacts $\varepsilon = 0{\cdot}1$ nm/D_{50}. Therefore, the accumulation of plastic deformation near the terminal density consists of successive, individual contact events rather than evenly distributed plastic strains throughout the specimen.

(*d*) The changes in void ratio, damping ratio and constrained modulus reveal that repetitive K_0 loading results in denser, stiffer and less attenuating sand fabrics. All these changes are a function of the initial void ratio e_0 and the stress amplitude ratio $\Delta\sigma/\sigma_0$.

(*e*) Shear wave velocity–stress trends $V_s = \alpha(\sigma'_{mean}/\text{kPa})^{\beta}$ capture both contact behaviour and fabric changes. Data show that sands become stiffer (lower C_c), the α factor increases, the β exponent decreases and the soil fabric becomes less sensitive to stress changes after repetitive loading. The increase in shear wave velocity indicates a gradual increase in horizontal stress during repetitive loading under zero lateral strains.

(*f*) Changes in shear wave velocity and G_{max} track the evolution of the constrained modulus M during repetitive loading. The stiffness ratio ranges between $1{\cdot}2 \leq M/G_{max} \leq 2{\cdot}3$ (lower values apply to denser specimens). Then, the maximum stiffness G_{max} computed from the shear wave velocity can be effectively used to estimate the elastic cyclic deformation in a given cycle.

(*g*) The maximum settlement a layer may experience when subjected to repetitive mechanical loads is a function of the initial and terminal void ratios. Data gathered in this experimental programme suggest a simple procedure to estimate the maximum settlement based on the initial and the minimum void ratios ($e_0 - e_{min}$) and the cyclic stress ratio $\Delta\sigma/\sigma_0$.

ACKNOWLEDGEMENTS

Support for this research was provided by the Kaust Endowment at King Abdullah University of Science and Technology. Gabrielle E. Abelskamp edited the manuscript.

NOTATION

a	slope in $\lambda - \Delta\sigma/\sigma_0$ plot $[(e_T - e_{min})/(e_0 - e_{min})]/(\Delta\sigma/\sigma_0)$
B	model parameter for maximum change in relative density
C_c	compression index
D	damping ratio
$D_{i=0}$	initial relative density at $i = 0$
D_r	relative density
D_{50}	median grain size
d	exponent in V_s–number of cycles relationship
E_{max}	small-strain Young's modulus
E_r	resilient modulus
e_i	void ratio at the number of cycles, i
e_{in}	void ratio after sample preparation
e_{max}	maximum void ratio
e_{min}	minimum void ratio
e_0	initial void ratio at the number of cycles, $i = 0$
e_T	terminal void ratio
e_1	void ratio at the end of first monotonic loading
G_{max}	maximum shear stiffness
G_s	specific gravity
H	sediment thickness
i	number of cycles
K_0	coefficient of earth pressure at rest
M	constrained modulus ($\Delta\sigma_z/\Delta\varepsilon_z$)
M_{max}	constrained modulus computed from the shear wave velocity
m	fitting parameter in the modified strain accumulation model
N	maximum number of cycles
N^*	characteristic number of cycles
n	model parameter for maximum change in relative density
S_T	total settlement induced by repetitive loading
V_p	compressional wave velocity
V_s	shear wave velocity
W	stored energy
z	depth
α	shear wave velocity at mean effective stress $\sigma'_{mean} = 1$ kPa
β	exponent in a power function of V_s–σ'_{mean} relationship
γ	shear strain
ΔD_T	maximum change in relative density induced by repetitive loads
Δe	change in void ratio
ΔW	consumed energy
$\Delta\sigma$	stress amplitude
$\Delta\sigma/\sigma_0$	stress amplitude ratio
ε^{pl}	plastic strain computed from two consecutive cycles
ε_{pp}	peak-to-peak strain
ε_T	maximum cumulative strain as $i \rightarrow \infty$
$\varepsilon_{th}\|^{el}$	elastic threshold strain
$\varepsilon_{th}\|^{v}$	volumetric threshold strain
ε_z	vertical strain
η	fraction of the ultimate compaction induced by repetitive loads
θ	stretching factor
λ	dimensionless volume contraction $[(e_T - e_{min})/(e_0 - e_{min})]$
ν	Poisson ratio
ρ	mass density
σ_0	vertical stress at the number of cycle $i = 0$
σ_y	yield stress
σ'_{mean}	mean effective stress on the polarisation plane
σ'_x	horizontal effective stress
σ'_z	vertical effective stress

REFERENCES

Achmus, M., Kuo, Y. S. & Abdel-Rahman, K. (2009). Behavior of monopile foundations under cyclic lateral load. *Comput. Geotech.* **36**, No. 5, 725–735.

Alarcon-Guzman, A., Leonards, G. A. & Chameau, J. L. (1988). Undrained monotonic and cyclic strength of sands. *J. Geotech. Engng* **114**, No. 10, 1089–1109.

Albrecht, B. A. & Benson, C. H. (2001). Effect of desiccation on compacted natural clays. *J. Geotech. Geoenviron. Engng* **127**, No. 1, 67–75.

Alonso, E. E., Romero, E., Hoffmann, C. & García-Escudero, E. (2005). Expansive bentonite–sand mixtures in cyclic controlled-suction drying and wetting. *Engng Geol.* **81**, No. 3, 213–226.

Alonso-Marroquin, F. & Herrmann, H. J. (2004). Ratcheting of granular materials. *Phys. Rev. Lett.* **92**, No. 5, 054301.

Andersen, K. H. (2009). Bearing capacity under cyclic loading-offshore, along the coast, and on land. *Can. Geotech. J.* **46**, No. 5, 513–535.

Barden, L. & Khayatt, A. J. (1966). Incremental strain rate ratios and strength of sand in the triaxial test. *Géotechnique* **16**, No. 4, 338–357, https://doi.org/10.1680/geot.1966.16.4.338.

Boulon, M. & Foray, P. (1986). Physical and numerical simulation of lateral shaft friction along offshore piles in sand. In *Proceedings of the 3rd international conference on numerical methods in offshore piling*, pp. 127–147. Paris, France: Editions Techrig.

Brown, S. F. (1974). Repeated load testing of a granular material. *J. Geotech. Engng Div., ASCE* **100**, No. 7, 825–841.

Brown, S. F. (1996). Soil mechanics in pavement engineering. *Géotechnique* **46**, No. 3, 383–426, https://doi.org/10.1680/geot.1996.46.3.383.

Cha, M., Santamarina, J. C., Kim, H. S. & Cho, G. C. (2014). Small-strain stiffness, shear-wave velocity, and soil compressibility. *J. Geotech. Geoenviron. Engng* **140**, No. 10, 06014011.

Chamberlain, E. J., Iskandar, I. & Hunsicker, S. E. (1990). Effect of freeze–thaw cycles on the permeability and macrostructure of soils. *Cold Regions Res. Engng Lab.* **90**, No. 1, 145–155.

Chong, S. H. & Santamarina, J. C. (2016). Sands subjected to vertical repetitive loading under zero lateral strain: accumulation models, terminal densities, and settlement. *Can. Geotech. J.* **53**, No. 22, 2039–2046.

Collins, I. F., Wang, A. P. & Saunders, L. R. (1993). Shakedown theory and the design of unbound pavements. *Road Transp. Res.* **2**, No. 4, 28–39.

Cuéllar, P., Baeßler, M. & Rücker, W. (2009). Ratcheting convective cells of sand grains around offshore piles under cyclic lateral loads. *Granular Matter* **11**, No. 6, 379–390.

Cuéllar, P., Georgi, S., Baeßler, M. & Rücker, W. (2012). On the quasi-static granular convective flow and sand densification around pile foundations under cyclic lateral loading. *Granular Matter* **14**, No. 1, 11–25.

da Fonseca, A. V., Rios, S., Amaral, M. F. & Panico, F. (2013). Fatigue cyclic tests on artificially cemented soil. *Geotech. Testing J.* **36**, No. 2, 227–235.

Dai, S., Wuttke, F. & Santamarina, J. C. (2013). Coda wave analysis to monitor processes in soils. *J. Geotech. Geoenviron. Engng* **139**, No. 9, 1504–1511.

D'Appolonia, D. J. & D'Appolonia, E. E. (1967). Determination of the maximum density of cohesionless soils. In *Proceedings of the 3rd Asian regional conference on soil mechanics and foundation engineering, Haifa, September 25–28*, vol. 1, pp. 266–268. Jerusalem, Israel: Jerusalem Academic Press.

D'Appolonia, D. J., Whitman, R. V. & D'appolonia, E. E. (1969). Sand compaction with vibratory rollers. *J. Soil Mech. Found. Div., ASCE* **95**, No. 1, 263–284.

Daramola, O. (1980). On estimating K_0 for overconsolidated granular soils. *Géotechnique* **30**, No. 3, 310–313, https://doi.org/10.1680/geot.1980.30.3.310.

Davich, P., Labuz, J., Guzina, B. & Drescher, A. (2004). *Small strain and resilient modulus testing of granular soils.* Minneapolis, MN, USA: Minnesota Department of Transportation, University of Minnesota.

Desai, C. S., Drumm, E. C. & Zaman, M. M. (1985). Cyclic testing and modeling of interfaces. *J. Geotech. Engng* **111**, No. 6, 793–815.

Di Donna, A. & Laloui, L. (2015). Response of soil subjected to thermal cyclic loading: experimental and constitutive study. *Engng Geol.* **190**, 65–76.

Di Maio, C. (1996). Exposure of bentonite to salt solution: osmotic and mechanical effects. *Géotechnique* **46**, No. 4, 695–707, https://doi.org/10.1680/geot.1996.46.4.695.

Dobry, R., Ladd, R. S., Yokel, F. Y., Chung, R. M. & Powell, D. (1982). *Prediction of pore water pressure buildup and liquefaction of sands during earthquakes by the cyclic strain method. NBS Building science series 138*. Washington, DC, USA: US Department of Commerce, National Bureau of Standards.

Drnevich, V. P. & Richart, F. E. (1970). Dynamic prestraining of dry sand. *J. Soil Mech. Found. Div.* **96**, No. SM2, 453–469.

Georgiannou, V. N. & Konstadinou, M. (2014). Effects of density on cyclic behaviour of anisotropically consolidated Ottawa sand under undrained torsional loading. *Géotechnique* **64**, No. 4, 287–302, https://doi.org/10.1680/geot.13.P.090.

Georgiannou, V. N., Tsomokos, A. & Stavrou, K. (2008). Monotonic and cyclic behaviour of sand under torsional loading. *Géotechnique* **58**, No. 2, 113–124, https://doi.org/10.1680/geot.2008.58.2.113.

Guimaraes, M. S., Valdes, J. R., Palomino, A. M. & Santamarina, J. C. (2007). Aggregate production: fines generation during rock crushing. *Int. J. Miner. Processing* **81**, No. 4, 237–247.

Guo, L., Cai, Y., Jardine, R. J., Yang, Z. & Wang, J. (2018). Undrained behaviour of intact soft clay under cyclic paths that match vehicle loading conditions. *Can. Geotech. J.* **55**, No. 1, 90–106.

Huang, A. B. (2016). Characterization of silt/sand soils. *Aust. Geomech. J.* **51**, No. 4, 1–22.

Indraratna, B., Tennakoon, N., Nimbalkar, S. & Rujikiatkamjorn, C. (2013). Behaviour of clay fouled ballast under drained triaxial testing. *Géotechnique* **63**, No. 5, 410–419, https://doi.org/10.1680/geot.11.P.086.

Ishihara, K. (1996). *Soil behavior in earthquake geotechnics.* New York, NY, USA: Oxford University Press.

Jardine, R. J. (1991). The cyclic behaviour of offshore piles. In *Cyclic loading of soils* (eds M. P. O'Reilly and S. F. Brown), pp. 174–248. Glasgow, UK: Blackie and Son.

Johnson, K. L. (1955). Surface interaction between elastically loaded bodies under tangential forces. *Proc. R. Soc. Lond. A* **230**, No. 1183, 531–548.

Johnson, K. L. (1961). Energy dissipation at spherical surfaces in contact transmitting oscillating forces. *J. Mech. Engng Sci.* **3**, No. 4, 362–368.

Kelly, R. B., Houlsby, G. T. & Byrne, B. W. (2006). A comparison of field and laboratory tests of caisson foundations in sand and clay. *Géotechnique* **56**, No. 9, 617–626, https://doi.org/10.1680/geot.2006.56.9.617.

Ko, H. Y. & Scott, R. F. (1967). Deformation of sand in hydrostatic compression. *J. Soil Mech. Found. Div. ASCE* **93**, No. SM3, 137–156.

LeBlanc, C., Houlsby, G. T. & Byrne, B. W. (2010). Response of stiff piles in sand to long-term cyclic lateral loading. *Géotechnique* **60**, No. 2, 79–90, https://doi.org/10.1680/geot.7.00196.

Lee, J. S. & Santamarina, J. C. (2005). Bender elements: performance and signal interpretation. *J. Geotech. Geoenviron. Engng* **131**, No. 9, 1063–1070.

Li, W., Igoe, D. & Gavin, K. (2015). Field tests to investigate the cyclic response of monopiles in sand. *Proc. Instn Civ. Engrs – Geotech. Engng* **168**, No. 5, 407–421, https://doi.org/10.1680/jgeen.14.00104.

López-Querol, S. & Coop, M. R. (2012). Drained cyclic behaviour of loose Dogs Bay sand. *Géotechnique* **62**, No. 4, 281–289, https://doi.org/10.1680/geot.8.P.105.

Loria, A. F. R., Gunawan, A., Shi, C., Laloui, L. & Ng, C. W. (2015). Numerical modelling of energy piles in saturated sand subjected to thermo-mechanical loads. *Geomech. Energy Environ.* **1**, 1–15.

Luong, M. P. (1980). Stress–strain aspects of cohesionless soils under cyclic and transient loading. *Proceedings of the international symposium on soils under cyclic and transient loading* (eds G. N. Pande and O. C. Zienkiewicz), pp. 315–324. Rotterdam, the Netherlands: Balkema.

Mayne, P. W. & Kulhawy, F. H. (1982). K_0–OCR relationships in soil. *J. Soil Mech. Found. Div.* **108**, No. 6, 851–872.

Monismith, C. L. (2004). Evolution of long-lasting asphalt pavement design methodology: a perspective. *Proceedings of*

international symposium on design and construction of long lasting asphalt pavements, Auburn, AL, USA.

Monismith, C. L., Ogawa, N. & Freeme, C. R. (1975). Permanent deformation characteristics of subgrade soils due to repeated loading. *Transpn Res. Rec.*

Musso, G., Morales, E. R., Gens, A. & Castellanos, E. (2003). The role of structure in the chemically induced deformations of FEBEX bentonite. *Appl. Clay Sci.* **23**, No. 1, 229–237.

Nakata, Y., Kajiwara, T. & Yoshimoto, N. (2013). Collapse behavior of slope due to change in pore water pressure. In *Proceedings of the 18th international conference on soil mechanics and geotechnical engineering: challenges and innovations in geotechnics* (eds P. Delage, J. Desrues, R. Frank, A. Puech and F. Schlosser), pp. 2225–2228. Paris, France: Presses des Ponts.

Narsilio, A. & Santamarina, J. C. (2008). Terminal densities. *Géotechnique* **58**, No. 8, 669–674, https://doi.org/10.1680/geot.2008.58.8.669.

NCHRP (National Cooperative Highway Research Program) (2004). *Guide for mechanistic-empirical design of new and rehabilitated pavement structures*. Washington, DC, USA: Transportation Research Board, National Research Council.

Omidvar, M., Iskander, M. & Bless, S. (2012). Stress–strain behavior of sand at high strain rates. *Int. J. Impact Engng* **49**, 192–213.

Orense, R., Farooq, K. & Towhata, I. (2004). Deformation behavior of sandy slopes during rainwater infiltration. *Soils Found.* **44**, No. 2, 15–30.

Papadopoulos, E. (2014). *Performance of unbound aggregate bases and implications for inverted base pavements*. PhD thesis, Georgia Institute of Technology, Atlanta, GA, USA.

Park, J. (2018). *Long-term response of soils subjected to repetitive mechanical loads: engineering implications*. PhD thesis, Georgia Institute of Technology, Atlanta, GA, USA.

Pasten, C. & Santamarina, J. C. (2011). Energy geo-storage–analysis and geomechanical implications. *KSCE J. Civ. Engng* **15**, No. 4, 655–667.

Pasten, C. & Santamarina, J. C. (2014). Thermally induced long-term displacement of thermoactive piles. *J. Geotech. Geoenviron. Engng* **140**, No. 5, 06014003.

Pasten, C., Shin, H. & Santamarina, J. C. (2014). Long-term foundation response to repetitive loading. *J. Geotech. Geoenviron. Engng* **140**, No. 4, 04013036.

Paute, J. L., Hornych, P. & Beraben, J.-P. (1993). Repeated load triaxial testing of granular materials on the French network of Laboratoires des Ponts et Chaussees. In *Flexible pavements: proceedings of the European symposium Euroflex 1993* (ed. A. Gomes Correia), pp. 53–64. Rotterdam, the Netherlands: AA Balkema.

Peng, J., Clarke, B. G. & Rouainia, M. (2006). A device to cyclic lateral loaded model piles. *Geotech. Testing J.* **29**, No. 4, 341–347.

Poulos, H. G. (1989). Cyclic axial loading analysis of piles in sand. *J. Geotech. Engng* **115**, No. 6, 836–852.

Qi, J., Ma, W. & Song, C. (2008). Influence of freeze–thaw on engineering properties of a silty soil. *Cold Reg. Sci. Technol.* **53**, No. 3, 397–404.

Roberts, J. E. & de Souza, J. M. (1958). The compressibility of sands. *Proc. Am. Soc. Testing Mater.* **58**, 1269–1272.

Rowe, P. W. (1954). A stress–strain theory for cohesionless soil with applications to earth pressures at rest and moving walls. *Géotechnique* **4**, No. 2, 70–88, https://doi.org/10.1680/geot.1954.4.2.70.

Sánchez, M., Shastri, A. & Le, T. M. H. (2014). Coupled hydromechanical analysis of an underground compressed air energy storage facility in sandstone. *Géotechnique Lett.* **4**, No. 2, 157–164, https://doi.org/10.1680/geolett.13.00068.

Santamarina, J. C. & Fratta, D. (2005). *Discrete signals and inverse problems: an introduction for engineers and scientists*. Chichester, UK: John Wiley & Sons.

Santamarina, J. C., Klein, K. A. & Fam, M. A. (2001). *Soils and waves: particulate materials behavior, characterization and process monitoring*. Chichester, UK and New York, NY, USA: J. Wiley & Sons.

Sawicki, A. & Swidzinski, W. (1995). Cyclic compaction of soils, grains and powders. *Powder Technol.* **85**, No. 2, 97–104.

Schuettpelz, C. C., Fratta, D. & Edil, T. B. (2010). Mechanistic corrections for determining the resilient modulus of base course materials based on elastic wave measurements. *J. Geotech. Geoenviron. Engng* **136**, No. 8, 1086–1094.

Sharp, R. W. & Booker, J. R. (1984). Shakedown of pavements under moving surface loads. *J. Transp. Engng* **110**, No. 1, 1–14.

Shenton, M. J. (1978). Deformation of railway ballast under repeated loading conditions. In *Railroad track mechanics and technology* (ed. A. D. Kerr), pp. 405–425. Oxford, UK: Pergamon Press.

Silver, M. L. & Seed, H. B. (1971). Volume changes in sands during cyclic loading. *J. Soil Mech. Found. Div.* **97**, No. 9, 1171–1182.

Snieder, R. (2006). The theory of coda wave interferometry. *Pure Appl. Geophys.* **163**, No. 2-3, 455–473.

Stokoe, K. H., Darendeli, M. B., Andrus, R. D. & Brown, L. T. (1999). Dynamic soil properties: laboratory, field and correlation studies. *Proceedings of the 2nd international conference on earthquake geotechnical engineering*, Lisbon, Portugal, vol. 3, pp. 811–846. Rotterdam, the Netherlands: Balkema.

Talesnick, M. L. (2012). A different approach and result to the measurement of K_0 of granular soils. *Géotechnique* **62**, No. 11, 1041–1045, https://doi.org/10.1680/geot.11.P.009.

Tatsuoka, F., Toki, S., Miura, S., Kato, H., Okamoto, M., Yamada, S. I., Yasuda, S. & Tanizawa, F. (1986). Some factors affecting cyclic undrained triaxial strength of sand. *Soils Found.* **26**, No. 3, 99–116.

Triantafyllidis, T., Wichtmann, T. & Niemunis, A. (2004). On the determination of cyclic strain history. In *Cyclic behaviour of soils and liquefaction phenomena* (ed. T. Triantafyllidis), pp. 321–332. London, UK: AA Balkema, Taylor & Francis Group.

Tripathy, S. & Rao, K. S. S. (2009). Cyclic swell–shrink behaviour of a compacted expansive soil. *Geotech. Geol. Engng* **27**, No. 1, 89–103.

Uesugi, M., Kishida, H. & Tsubakihara, Y. (1989). Friction between sand and steel under repeated loading. *Soils Found* **29**, No. 3, 127–137.

Valdes, R. (2002). *Fines migration and formation damage: microscale studies*. PhD thesis, Georgia Institute of Technology, Atlanta, GA, USA.

Viklander, P. (1998). Permeability and volume changes in till due to cyclic freeze/thaw. *Can. Geotech. J.* **35**, No. 3, 471–477.

Vucetic, M. (1994). Cyclic threshold shear strains in soils. *J. Geotech. Engng* **120**, No. 12, 2208–2228.

Vucetic, M. & Dobry, R. (1991). Effect of soil plasticity on cyclic response. *J. Geotech. Engng* **117**, No. 1, 89–107.

Werkmeister, S., Dawson, A. R. & Wellner, F. (2005). Permanent deformation behaviour of granular materials. *Road Mater. Pavement* **6**, No. 1, 31–51.

White, D. J. & Lehane, B. M. (2004). Friction fatigue on displacement piles in sand. *Géotechnique* **54**, No. 10, 645–658, https://doi.org/10.1680/geot.2004.54.10.645.

Whitman, R. V. (1970). *The response of soils to dynamic loadings*, Report 26, Final report. Cambridge, MA, USA: Department of Civil Engineering, Massachusetts Institute of Technology.

Wichtmann, T. (2005). *Explicit accumulation model for non-cohesive soils under cyclic loading*. PhD thesis, Inst. für Grundbau und Bodenmechanik, Braunschweig, Germany.

Wichtmann, T., Niemunis, A. & Triantafyllidis, T. (2005). Strain accumulation in sand due to cyclic loading: drained triaxial tests. *Soil. Dyn. Earthq. Eng* **25**, No. 12, 967–979.

Wichtmann, T., Rondón, H. A., Niemunis, A., Triantafyllidis, T. & Lizcano, A. (2010a). Prediction of permanent deformations in pavements using a high-cycle accumulation model. *J. Geotech. Geoenviron. Engng* **136**, No. 5, 728–740.

Wichtmann, T., Niemunis, A. & Triantafyllidis, T. (2010b). On the determination of a set of material constants for a high-cycle accumulation model for non-cohesive soils. *Int. J. Numer. Analyt. Methods Geomech.* **34**, No. 4, 409–440.

Wichtmann, T., Niemunis, A. & Triantafyllidis, T. (2010c). Strain accumulation in sand due to drained cyclic loading: on the effect of monotonic and cyclic preloading (Miner's rule). *Soil Dynamics Earthquake Engng* **30**, No. 8, 736–745.

Wu, T., Cai, Y., Guo, L., Ling, D. & Wang, J. (2017). Influence of shear stress level on cyclic deformation behaviour of intact

Wenzhou soft clay under traffic loading. *Engng Geol.* **228**, 61–70.
Youd, T. L. (1970). Densification and shear of sand during vibration. *J. Soil Mech. Found. Div, ASCE* **96**, No. 3, 863–880.
Youd, T. L. (1972). Compaction of sands by repeated shear straining. *J. Soil Mech. Found. Div, ASCE* **98**, No. SM7, 709–725.
Yu, P. & Richart, F. E. Jr (1984). Stress ratio effects on shear modulus of dry sands. *J. Geotech. Engng* **110**, No. 3, 331–345.